Israel Journal of Chemistry

DOI: 10.1002/ijch.201200067

Synthesis and Photocatalytic Properties of Single Crystalline $(Ga_{1-x}Zn_x)(N_{1-x}O_x)$ Nanotubes

Christopher Hahn,[a, b] Melissa A. Fardy,[a, b] Catherine Nguyen,[a] Michelle Natera-Comte,[a, c] Sean C. Andrews,[a, b] and Peidong Yang*[a, b]

Abstract: Recently, $(Ga_{1-x}Zn_x)(N_{1-x}O_x)$ has gained widespread attention as a comparatively high efficiency photocatalyst for visible-light-driven overall water splitting. Despite significant gains in efficiency over the past several years, a majority of the photogenerated carriers recombine within bulk powders. To improve the photocatalytic activity, we used an epitaxial casting method to synthesize single-crystalline, high surface area $(Ga_{1-x}Zn_x)(N_{1-x}O_x)$ nanotubes with ZnO compositions up to $x = 0.10$. Individual nanotubes showed improved homogeneity over powder samples due to a well defined epitaxial interface for ZnO diffusion into GaN. Absorption measurements showed that the ZnO incorporation shifts the absorption into the visible region with a tail out to 500 nm. Gas chromatography (GC) was used to compare the solar water splitting activity of $(Ga_{1-x}Zn_x)(N_{1-x}O_x)$ nanotubes ($x = 0.05$–0.10) with similar composition powders. Co-catalyst decorated samples were dispersed in aqueous solutions of CH_3OH and AgO_2CCH_3 to monitor the H^+ reduction and H_2O oxidation half reactions, respectively. The nanotubes were found to have approximately 1.5–2 times higher photocatalytic activity than similar composition powders for the rate limiting H^+ reduction half reaction. These results demonstrate that improvements in homogeneity and surface area using the nanotube geometry can enhance the photocatalytic activity of GaN:ZnO for solar water splitting.

Keywords: alloy · nanotube · oxynitride · photocatalyst · water splitting

1 Introduction

Sunlight is a clean and renewable energy source, which could ultimately help meet the world's energy needs. However, the large variations in solar flux present a significant barrier for on-demand energy supply. A storage method to solve this issue is the conversion of solar energy into the chemical bonds of a fuel. One such fuel source is hydrogen, which has a lot of appeal due to its high energy density (140 kJ/gram) and clean emissions ($H_2 + O_2 \rightarrow H_2O +$ electricity).[1] Although solar energy can be converted into hydrogen by coupling photovoltaic cells to electrolyzers, the current cost of electrolyzers prevents the large scale implementation of such a method.[2] Therefore, researchers are investigating the direct photolysis of water on a semiconductor surface, the so called "Holy Grail" of solar energy conversion.[3]

To perform efficient photolysis of water (water splitting) under sunlight, a semiconductor must: (a) absorb a large fraction of sunlight in the visible region (band gap around 2.0 eV), (b) straddle the H^+/H_2 reduction and H_2O/O_2 oxidation potentials with its conduction and valence bands, (c) be stable under water splitting conditions, and (d) effectively separate photogenerated carriers and transport them to the surface.[3] Typical II/VI, III/V, and group IV materials can satisfy criteria (a) and (d), which are analogous to requirements for producing efficient photovoltaic cells. To date, these systems have generated the highest efficiencies for photoelectrochemical (PEC) water splitting.[4] However, these same materials generally have problems with photocorrosion[5],[6] and/or the energetic requirements for spontaneous water splitting.[7] There are several metal oxides, most notably TiO_2,[8] that have the proper band positions, photostability, and a high internal quantum efficiency (IQE). However, their ultraviolet (UV) band gaps lead to poor light absorption, which prevents them from reaching a high solar to hydrogen efficiency under sunlight. Metal oxides typically have

[a] C. Hahn,[+] M. A. Fardy,[+] C. Nguyen, M. Natera-Comte, S. C. Andrews, P. Yang
Department of Chemistry, University of California, Berkeley, California 94720
phone: +510 643 1545
fax: +510 642 7301
e-mail: p_yang@berkeley.edu

[b] C. Hahn,[+] M. A. Fardy,[+] S. C. Andrews, P. Yang
Materials Sciences Division, Lawrence Berkeley National Laboratory, Berkeley, California 94720

[c] M. Natera-Comte
Technische Physik, University of Würzburg, Am Hubland, 97074 Würzburg, Germany

[+] These authors contributed equally to this work.

Supporting information for this article is available on the WWW under http://dx.doi.org/10.1002/ijch.201200067.

a large potential difference between their valence band potential and the water oxidation potential because their valence bands are comprised mostly of low energy O 2p orbitals. Therefore, one strategy to reduce the band gap of metal oxides is to substitute oxygen with anions with higher energy p orbitals such as N (oxynitrides) and S (oxysulfides).[9]

In 2005, K. Maeda et al. discovered that the solid solution of GaN and ZnO [$(Ga_{1-x}Zn_x)(N_{1-x}O_x)$, denoted as GaN : ZnO] could effectively reduce the band gap of both starting materials.[10] Although both GaN and ZnO have band gaps in the UV region, the absorption tail of GaN : ZnO may be tuned from 3.4 to 2.43 eV by increasing the ZnO composition from 0 to 42 %.[11] Despite a shift in the valence band maximum from Zn acceptor levels, GaN : ZnO can still spontaneously split water because the conduction band minimum and the valence band maximum straddle the H^+/H_2 reduction and H_2O/O_2 oxidation potentials, respectively. When decorated with a $Rh_{2-y}Cr_yO_3$ co-catalyst, powder GaN : ZnO photocatalysts achieved a quantum efficiency (QE) of 5.9 % for overall water splitting at 420–440 nm.[12]

Despite the significant improvements made to GaN : ZnO powders by optimizing the preparation and treatment conditions, the IQE is still limited by the recombination of photogenerated carriers. Factors that dictate the IQE for water splitting are the efficiency of interfacial charge transfer and charge transport to the solid-liquid interface.[13] Much work has been done to optimize the interfacial charge transfer efficiency for GaN : ZnO by using co-catalysts,[14] so instead we will discuss improving charge transport to the solid-liquid interface. One limitation for efficient charge transport within GaN : ZnO powders is phase inhomogeneities, which can trap and localize photogenerated charges. These ZnO rich regions are formed during the simultaneous solid state diffusion of ions at random solid-solid boundaries in the powder mixture.[11] Therefore, a more homogeneous product could be obtained by increasing the solid-solid contact area between precursors during solid state diffusion. Another limitation is the small fraction of active region for water splitting due to the typical grain sizes[11] of GaN : ZnO powders. Photogenerated charges outside of the active region (sum of the minority carrier diffusion length and depletion width) will recombine before reaching the surface. Therefore, decreasing the size of GaN : ZnO through nanostructuring could allow for more efficient charge transport to the solid-electrolyte interface. In particular, the nanotube geometry has shown great potential for water splitting,[15],[16] due to its comparatively large active region and solid-electrolyte interface.

In 2003, Goldberger et al. reported the first synthesis of single-crystal GaN nanotube arrays by an epitaxial casting method.[17] Interfacial diffusion between the ZnO nanowire core and GaN shell during growth and template removal caused the resulting nanotubes to contain a small amount of Zn and O impurities. However, most of the ZnO was removed by prolonged heating under NH_3. Alternatively, this interfacial diffusion could be used to promote alloying at the ZnO-GaN interface to generate single-crystalline GaN : ZnO nanotubes. Since the ZnO-GaN interface is epitaxial, and therefore well defined for diffusion, an increase in homogeneity relative to powders could be expected. In addition, an increase in active region compared to GaN : ZnO powders could be obtained by controlling the thickness of nanotubes. Here we report the epitaxial casting of single-crystalline GaN : ZnO nanotubes and their photocatalytic properties for solar water splitting.

2 Structural Properties

GaN : ZnO nanotubes were synthesized using an epitaxial casting method, as seen in the schematic in Figure 1A. To construct nanowire films, a suspension of ZnO nanowires in ethanol was drop-cast onto a quartz substrate and dried at room temperature. Using metal organic chemical vapor deposition (MOCVD), the ZnO nanowire film was epitaxially coated with GaN, producing a network of core-shell nanowires. After etching of the ZnO nanowire cores at high temperature in NH_3 ambient, GaN : ZnO nanotubes formed. During the shell deposition and subsequent annealing procedure, interfacial diffusion between the ZnO core and GaN shell led to the generation of a GaN : ZnO alloy within the shell. Oriented nanotube arrays could be synthesized instead of films by starting with oriented arrays of ZnO nanowires (Figure S1–S2).

The morphology of a representative film (Figure 1B–D) was examined through each step of the synthetic process by using scanning electron microscopy (SEM). A top down image of the ZnO nanowire film (Figure 1B) shows that the wires have lengths of 3–5 μm. The nanowires also tended to bundle, causing contact among wires at several points. After GaN shell deposition (Figure 1C), the nanowires clearly increased in diameter, although there was some merging of nanowires due to their proximity. After removal of the ZnO core (Figure 1D) in a high temperature ammonia environment, no sintering of nanotubes could be seen. A close up image reveals that the resulting GaN : ZnO nanotubes are hexagonally faceted with open tips (Figure 2A, Figure S2A). The tips most likely open due to a discrepancy in GaN growth on the polar (tip) vs non-polar (side walls) ZnO nanowire facets during the shell deposition. The open tips are necessary to move electrolyte freely into the nanotubes, allowing both the inner and outer surfaces to participate in water splitting. A low magnification transmission electron microscope (TEM) image (Figure 2B) of GaN : ZnO nanotubes confirms that the ZnO core has been removed. Typical inner diameters were measured to be 40–60 nm with wall thicknesses of ~20 nm. The inner diameter and wall thickness

Israel Journal of Chemistry

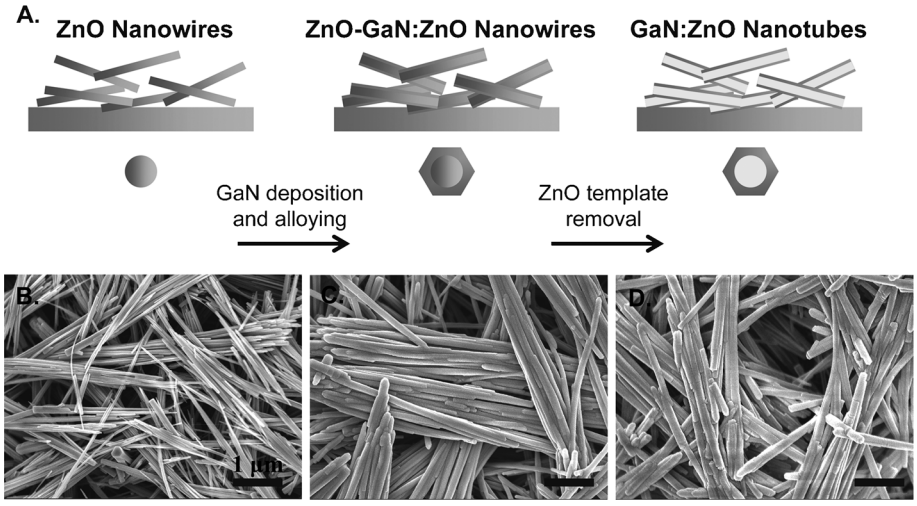

Figure 1. A) Schematic showing the epitaxial casting procedure used to generate GaN : ZnO nanotube films. B–D) SEM images of films consisting of B) ZnO nanowires, C) ZnO-GaN : ZnO core-shell nanowires, and D) GaN : ZnO nanotubes.

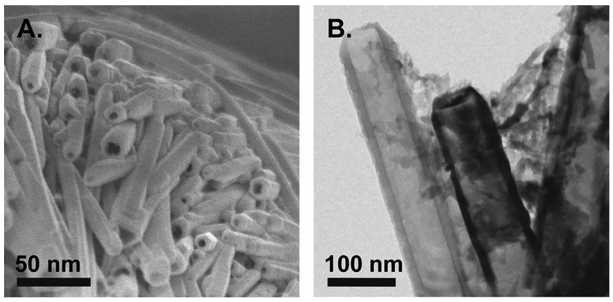

Figure 2. A) A close up SEM image showing that GaN : ZnO nanotubes are hexagonally faceted and have open tips. B) A low magnification TEM image confirms that the nanotubes have open tips and are hollow.

could be controlled by the core diameter and GaN deposition time, respectively. Some extraneous material can be seen from broken nanotube pieces that formed during the sonication process, which was performed in order to remove the nanotubes from the substrate.

Structural characteristics of GaN : ZnO nanotubes were investigated using X-ray diffraction (XRD) and high resolution TEM (HRTEM). An XRD pattern (Figure 3A) of a representative GaN : ZnO nanotube film shows diffraction peaks which can be assigned to the wurtzite crystal structure. Hexagonal lattice constants $a = 3.21$ Å and $c = 5.20$ Å were calculated from the 100 and 002 peaks respectively, which are shifted between those of wurtzite GaN and ZnO. No pure GaN or ZnO peaks were seen in the XRD pattern, indicating the formation of a solid solution of GaN and ZnO. A HRTEM image (Figure 3B) indicates that the epitaxial casting approach was successful in generating single-crystalline GaN : ZnO nanotubes.

The composition and homogeneity of $(Ga_{1-x}Zn_x)(N_{1-x}O_x)$ nanotubes were studied using TEM energy dispersive x-ray spectroscopy (EDS). A representative EDS spectrum (Figure 3C) shows that the nanotube has both Ga and Zn with a ZnO composition of 10 % ($x = 0.10$). Different nanotubes from the same sample had a composition range between 5–10 % ($x = 0.05$–0.10). Point measurements taken at different locations on the same nanotube had a standard deviation of only 1.3 %, indicating a higher degree of composition uniformity, compared to grains of bulk powders, which are mixed and reacted.[11] We believe the well defined core-shell epitaxial interface allows for more uniform diffusion of ZnO into GaN. An EDS line scan across the diameter of a nanotube (Figure 3D) confirms that Ga, Zn, N, and O are distributed homogeneously. The dip in intensity at the center for Ga, Zn, N, and O is characteristic of hollow nanotube geometry, and shows that the core has been completely removed.

3 Optical Properties

Absorption measurements were conducted to determine whether alloying shifts the band gap energy of GaN : ZnO nanotubes. Samples were prepared on double-sided polished quartz as a transparent substrate for the measurement. An integrating sphere was used for the absorption measurement, due to the large amount of scattering in the films. Both reflection (R) and transmission (T) geometries were used to calculate the absorption (A) percent, using the equation $A = 100 - R - T$. The calculated absorption percent of a film after each step of the epitaxial casting process is shown in Figure 4. Compared to the starting ZnO nanowires the ZnO-GaN : ZnO core-shell nanowires and GaN : ZnO nanotubes show a significant increase in visible absorption extending out to ~500 nm. This shift in the absorption edge is similar to the results reported by Maeda et al. for GaN : ZnO samples with 5–

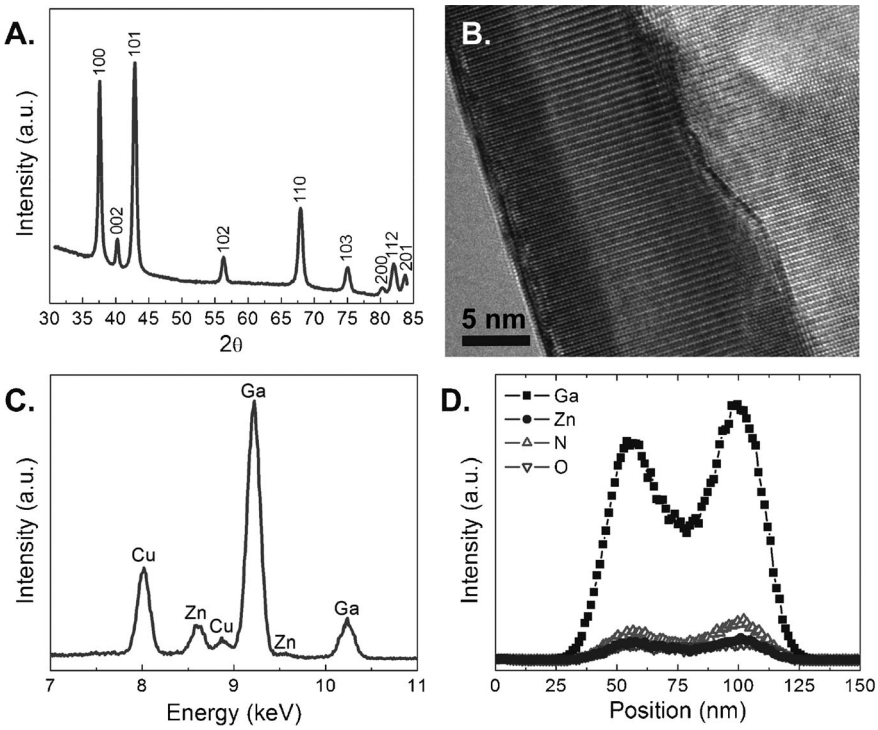

Figure 3. A) The XRD pattern of a GaN:ZnO nanotube film shows a wurtzite crystal structure, corresponding to a solid solution of GaN and ZnO. B) An HRTEM image shows that the GaN:ZnO nanotubes are single crystalline. C) A representative EDS spectrum shows that there is residual Zn within the nanotubes and D) an EDS line scan across the diameter of the nanotube shows that Ga, Zn, N, and O are distributed evenly.

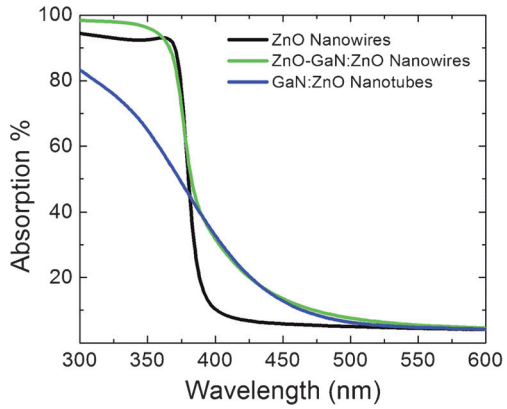

Figure 4. Absorption spectra of ZnO nanowires (black), ZnO-GaN:ZnO core-shell nanowires (green), and $(Ga_{1-x}Zn_x)(N_{1-x}O_x)$ nanotubes (blue), where x = 0.05–0.10. Visible light absorption ($\lambda >$ 400 nm) was observed for both the core-shell nanowires and the nanotubes.

10% ZnO.[11] Since both ZnO-GaN:ZnO core-shell nanowires and GaN:ZnO nanotubes display similar absorption spectra at $\lambda > 400$ nm, we believe that most of the diffusion happens during epitaxy, rather than during the core etching process. In addition, GaN:ZnO nanotubes show a gradual increase in absorption with decreasing wavelength, rather than the abrupt transition seen with the pure ZnO nanowires which is typical for direct band gap semiconductors. This band tail shows that the increase in visible light absorption most likely comes from ZnO impurity levels in GaN, rather than a change in the intrinsic band edge.[18]

4 Photocatalytic Activity

Photocatalytic experiments were conducted on GaN:ZnO nanotubes using sacrificial reagents to monitor each water splitting half reaction. To compare activities, standard GaN:ZnO powders with a stoichiometric ratio (5–10% ZnO, x = 0.05–0.10) equivalent to that of the nanotubes were synthesized (Figure S3) and calcined, according to the method of K. Maeda et al.[10] Previous reports on GaN:ZnO powders showed that negligible amounts of H_2 and O_2 were detected in overall water splitting experiments when no co-catalyst was used for the reduction reaction.[19] Recently, high water reduction activities with GaN:ZnO powders have been reported when Rh-Cr_2O_3 core-shell nanoparticle co-catalysts were used.[20] Using a modified two step photodeposition method,[21] Rh-Cr_2O_3 nanoparticles were deposited on both GaN:ZnO nanotube and powder samples, with the same experimental conditions in both cases. A high-angle annular dark-field (HAADF) scanning TEM (STEM) image shows the uniform decoration of particles on a nanotube surface (Figure S4A). Elemental analysis using EDS showed that nanotubes had 2.3% (wt) Rh and

0.9% Cr, while the powder had 1.6% Rh and 0.6% Cr. With similar particle densities, a higher wt% is expected for the nanotubes, due to a larger surface to volume ratio.

To monitor the water reduction half reaction, CH_3OH (MeOH) was used as a sacrificial reagent, since it is thermodynamically easier to oxidize than water and will oxidize irreversibly. Dried Rh-Cr_2O_3 loaded samples were dispersed in an aqueous 10% MeOH solution and illuminated with visible light ($\lambda > 400$ nm, 200 mW/cm^2 light intensity) from a 450 W Xe lamp. A GC was used to measure the evolved gas from a batch reactor cell, placed within a glove box. After an initial induction period (2 hrs), both nanotube and powder samples displayed an increase in total H_2 production (Figure 5A). This short induction period could be due to reduction of any unreacted Cr(VI) into Cr(III),[22] which would lower the H^+ reduction activity. After 2 hrs, a steady decrease in H_2 evolution rate was observed for both nanotube and powder samples. Previous studies on Rh-Cr photodeposits[20] showed similar trends for H_2 evolution, due to the instability of the Rh metal core. The H^+ reduction activity was compared for nanotube and powder samples by normalizing the total gas generated (μmol) to the amount of photocatalyst (g). After the induction period, nanotubes were found to generate H_2 at a rate 1.5–2 times higher than the powder samples.

Next, the water oxidation reaction was examined by using AgO_2CCH_3 (AgAc) as a sacrificial reagent. Although high activities for water oxidation with GaN:ZnO powders have been previously reported without an oxidation co-catalyst,[23] no activity was observed for bare GaN:ZnO nanotubes. This could be due to a difference in synthetic methods, since low temperature MOCVD products, such as our nanotules, have been reported to incorporate a large amount of carbon and hydrogen originating from the metal-organic precursor.[24] These impurities can accumulate at the surface, causing Fermi level pinning,[25] and adding radiative recombination centers.[26] To help increase charge separation and improve the photocatalytic activity of the surface, IrO_x nanoparticles were mixed and deposited on the nanotubes, as a water oxidation co-catalyst. A HAADF STEM image shows that the brightly contrasted IrO_x nanoparticles tend to aggregate into rod shaped features (Figure S4B). The same method was applied to the powder samples in order to directly compare water oxidation activities. EDS measurements showed that nanotubes had 2.9% Ir loading, while the powder had 1.3%. Samples were dispersed in 0.01 M AgAc aqueous solutions and illuminated with the previously described geometry and visible light intensity. After 2 hrs of illumination, the nanotube and powder samples showed similar O_2 levels (Figure 5B). However, after 4 hrs, the activity of the nanotubes steeply declined, while the activity of the powder only decreased slightly. No additional N_2 was detected beyond a small leak into the cell, indicating that both nanotube and powder samples were stable to photooxidation during the measurement.

An examination of powder and nanotube samples from the GC reactor, using TEM and EDS, shows that Ag particles were formed from the reduction of the Ag(I) sacrificial reagent during the experiment (Figure S5). Deposition of metallic Ag on the surface can reduce the activity of photocatalysts by increasing carrier recombination, blocking light absorption, and obstructing active sites.[23] While large Ag particles appeared to nucleate on the surface of the nanotubes (Figure S5A), it was difficult to distinguish between the Ag particles and GaN:ZnO powder (Figure S5B), which have similar morphologies. Instead, EDS experiments were conducted to compare the total amount of Ag deposited for the two geometries. Nanotubes were found to have 34.1% (wt) Ag, whereas the powder only had 5.5%. While it is not completely understood why Ag particles preferentially nucleated on the nanotubes, we believe this to be the primary reason for the faster deactivation of the nanotube photocatalysts.

Previous reports have shown that the H^+ reduction reaction could be the rate limiting step for overall water splitting with GaN:ZnO and other oxynitride systems.[9] This suggests that an improvement in the H^+ reduction activity would increase the overall water splitting activity.

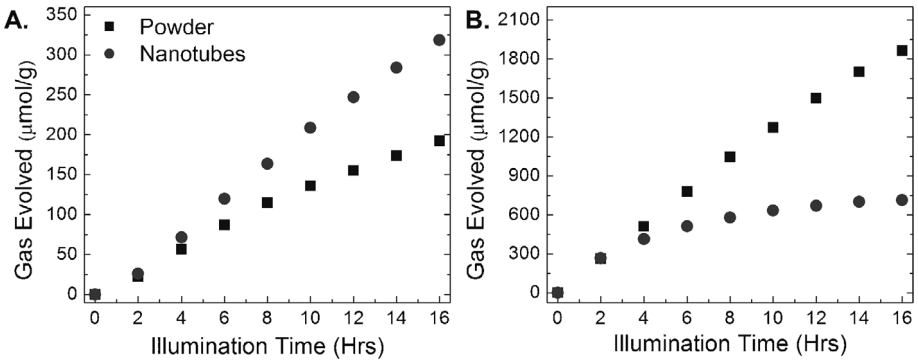

Figure 5. A) Hydrogen evolution from Rh-Cr_2O_3 decorated $(Ga_{1-x}Zn_x)(N_{1-x}O_x)$ nanotubes and powder (x = 0.05–0.10). Nanotubes show greater H^+ reduction activity than the powder sample. B) Oxygen evolution from IrO_x decorated $(Ga_{1-x}Zn_x)(N_{1-x}O_x)$ nanotubes and powder (x = 0.05–0.10). Although the nanotube and powder samples have similar initial H_2O oxidation rates, the nanotubes deactivated more quickly due to a larger amount of Ag metal deposition on the surface.

Here, we have demonstrated a 1.5–2 times increase in H^+ reduction activity relative to micron sized GaN:ZnO powders, by using the nanotube geometry. We have also shown that co-catalyst decorated GaN:ZnO powders and nanotubes have similar activities for H_2O oxidation. Therefore, we propose that with a correct dispersion of reduction and oxidation co-catalysts, GaN:ZnO nanotubes can achieve a higher overall water splitting efficiency than GaN:ZnO powders of the same stoichiometry.

5 Conclusions

In conclusion, $(Ga_{1-x}Zn_x)(N_{1-x}O_x)$ nanotubes with compositions up to $x = 0.10$ were successfully synthesized using an epitaxial casting approach. Examination of the morphology of GaN:ZnO nanotubes showed that they have open tips and high surface areas for photocatalysis. Nanotubes have a wurtzite crystal structure and are single-crystalline due to the formation of a solid solution of GaN:ZnO. Local elemental analysis of single nanotubes showed that they are more homogeneous than the previously reported powder samples, due to a well defined epitaxial interface for diffusion. GC measurements showed that co-catalyst coated nanotubes have increased activity for H^+ reduction and similar activity for H_2O oxidation, relative to powder samples of similar ZnO composition. These results lead us to believe that the nanotube geometry can enhance the overall water splitting activity of GaN:ZnO systems, due to increased surface area and improved composition homogeneity. Future work will involve optimizing the loading of oxidation and reduction co-catalysts on the surface of GaN:ZnO nanotubes to achieve overall water splitting. Although the $(Ga_{1-x}Zn_x)(N_{1-x}O_x)$ compositions reported in this manuscript are within $x = 0.05$–0.10, the highest water splitting efficiencies reported have been for $x > 0.10$. Further work will be done with modifying growth temperatures and annealing experiments to increase the resulting ZnO composition of the nanotubes.

6 Experimental

Preparation of ZnO Nanowires: ZnO nanowires were synthesized using a method similar to that reported by Yuhas et al.[27] 0.486 g of anhydrous Zn acetate (Aldrich), 101 μL of oleic acid (99%), and 25 mL of trioctylamine (98%) were combined in a 50 mL single-neck, round bottom flask fitted with a condenser. The flask was lowered into a pre-heated silicone oil bath at 300° and heated under stirring. After about 90 minutes the flask was removed from the oil bath and allowed to cool to room temperature. The product was centrifuged and washed with ethanol 3 times.

Preparation of ZnO Nanowire Films: ZnO nanowire films were deposited on $1 \times 1\ cm^2$ double-polished quartz substrates. A ZnO nanowire solution was made using approximately 80 mg of dry ZnO nanowire powder suspended in 10 mL of ethanol (EtOH). Nanowires were sonicated for 60 minutes to break apart any bundles. The nanowire solution was drop-cast onto the quartz substrates and dried at room temperature to produce uniform films of ZnO nanowires.

Preparation of ZnO-GaN:ZnO Core-Shell Nanowires: GaN was deposited on the ZnO nanowires using MOCVD, similar to the method reported by Goldberger et al.[17] The deposition was carried out in a home-built system consisting of a tube furnace, which contains a 1-in outer quartz tube and a $^1/_4$-in inner quartz tube. The outer tube was used to deliver a flow of NH_3, while the inner tube was used to deliver flows of trimethylgallium (TMG) using N_2 as the carrier gas. The TMG was stored in a bubbler and cooled to −10.9°. Prior to the start of the reaction, the furnace was heated to 600° under a flow of 20 sccm NH_3. Once a temperature of 600° was reached, 5 sccm of N_2 were passed through the TMG bubbler. This flow was further diluted with 150 sccm of N_2 before reaching the inner tube. At the output of the inner tube, the TMG reacted with the NH_3, coating the ZnO nanowires with GaN. After a 90 second growth time, the TMG and NH_3 flows were switched off and the nanowires were cooled to room temperature under N_2 ambient.

Preparation of GaN:ZnO Nanotubes: The ZnO nanowire cores were etched away from the ZnO-GaN:ZnO core-shell nanowires to generate GaN:ZnO nanotubes. To etch the ZnO cores, the nanowires were heated at 700° under NH_3 for 30 min. The average ZnO composition of GaN:ZnO nanotubes could be tuned from 10 to 1 at % by controlling the NH_3 etch time between 30 min to 4 hrs. The resulting nanotube film was removed from the substrate by sonication in EtOH and dried, producing a powder of GaN:ZnO nanotubes. The powder was subsequently placed into a porcelain crucible and calcined at 600° for 1 hr inside a tube furnace.

Addition of Rh-Cr_2O_3 Co-catalysts: Rh-Cr_2O_3 core-shell nanoparticles were deposited using analogous conditions to a previously reported photodeposition method.[21] For the Rh photodeposition, approximately ~1.5 mg of nanotubes were suspended in 2 ml of 0.1 mM $Na_3RhCl_6 \cdot 12H_2O$ aqueous solution (Alfa Aesar, 17.1%) and 0.2 ml of MeOH, inside a 5 ml glass vial. This solution was stirred and purged by bubbling Ar gas. After 1 hr of purging, the nanotubes were illuminated for 15 min using a 300 W Xe lamp fitted with a diffuser for uniform light intensity. The intensity was measured to be $300\ mW/cm^2$ using a Melles Griot broadband power meter. To purify the Rh coated nanotubes, the solid was collected by centrifugation at 6000 RPM (30 min) and washed several times with water. For the Cr_2O_3 shell, the Rh coated nanotubes were suspended in 2 ml of 0.2 mM K_2CrO_4 aqueous solution (Alfa

Aesar, 99%) and 0.2 ml of MeOH, inside a 5 ml glass vial. The sample was also purged with Ar for 1 hr and illuminated for 15 min, using the same Xe lamp geometry. After purification, the samples were dried overnight in a vacuum oven at 70°.

Addition of IrO_x Co-catalysts: Ligand-free IrO_x nanoparticles were synthesized using a previously reported method.[28] Approximately ~1.5 mg of nanotubes were mixed with 1 ml of a pH 10 solution of the IrO_x nanoparticles inside a porcelain crucible and stirred for 1 hr. After the nanotubes settled to the bottom of the crucible, the supernatant was removed. The resulting solid was calcined within the crucible at 400° for 1 hr inside a tube furnace.

Photocatalysis Experiments: Photocatalytic reactions were carried out in a specially designed 13 ml quartz reactor. The dry co-catalyst coated nanotubes (~1.5 mg) were suspended in 3 ml of 10% MeOH or 0.01 M $AgC_2H_3O_2$ (Aldrich, 99.99%) aqueous solutions. The nanotubes were illuminated with a 450 W Xe lamp fitted with a water filter, diffuser, and a 400 nm longpass filter. The light intensity was measured to be 200 mW/cm^2, using a Melles Griot broadband power meter. Sample gases were analyzed using an Agilent micro GC with a TCD detector. The entire setup, including the reactor, GC, and gas delivery lines, was enclosed in an acrylic glovebox to prevent leakage of air into the reactor (Figure S6). Prior to the start of illumination, the electrolyte was degassed under vacuum and the headspace was filled with ~1000 torr of Ar (5N). During the course of the reaction, gas samples from the reactor headspace were periodically injected into the GC, and the pressures were recorded to determine the total amount of gas.

Characterization: SEM images were taken using a JEOL JSM 6340F field-emission SEM operating at 5 kV. XRD patterns were collected using a Bruker D8 GADDS diffractometer with Co k_α irradiation. TEM samples were prepared by sonicating the nanotube films into a solution of isopropanol and drop-casting the solution on lacey carbon support grids. The TEM images and EDS spectra were taken using the following instruments: a Tecnai G2 S-Twin TEM operating at 200 kV, a Philips CM200/FEG TEM operating at 200 kV, equipped with an Oxford INCA energy dispersive X-ray detector, and a JEOL JEM-2100 LaB_6 TEM operating at 200 kV, equipped with an Oxford INCA energy dispersive X-ray detector. Absorption measurements were collected using a Shimadzu UV-3101 PC, equipped with an ISR-3100 integrating sphere.

References

[1] Y. Li, J. Z. Zhang, *Laser Photonics Rev.* **2010**, *4* (4), 517–528.
[2] J. A. Turner, *Science* **1999**, *285* (5428), 687–689.
[3] M. G. Walter, E. L. Warren, J. R. McKone, S. W. Boettcher, Q. X. Mi, E. A. Santori, N. S. Lewis, *Chem. Rev.* **2010**, *110* (11), 6446–6473.
[4] O. Khaselev, J. A. Turner, *Science* **1998**, *280* (5362), 425–427.
[5] A. J. Bard, M. S. Wrighton, *J. Electrochem. Soc.* **1977**, *124* (11), 1706–1710.
[6] H. Gerischer, *J. Electroanal. Chem.* **1977**, *82* (1–2), 133–143.
[7] T. Bak, J. Nowotny, M. Rekas, C. C. Sorrell, *Int. J. Hydrog. Energy* **2002**, *27* (10), 991–1022.
[8] M. Ni, M. K. H. Leung, D. Y. C. Leung, K. Sumathy, *Renew. Sust. Energ. Rev.* **2007**, *11* (3), 401–425.
[9] K. Maeda, K. Domen, *J. Phys. Chem. C* **2007**, *111* (22), 7851–7861.
[10] K. Maeda, T. Takata, M. Hara, N. Saito, Y. Inoue, H. Kobayashi, K. Domen, *J. Am. Chem. Soc.* **2005**, *127* (23), 8286–8287.
[11] K. Maeda, K. Domen, *Chem. Mat.* **2010**, *22* (3), 612–623.
[12] K. Maeda, K. Teramura, K. Domen, *J. Catal.* **2008**, *254* (2), 198–204.
[13] Z. B. Chen, T. F. Jaramillo, T. G. Deutsch, A. Kleiman-Shwarsctein, A. J. Forman, N. Gaillard, R. Garland, K. Takanabe, C. Heske, M. Sunkara, E. W. McFarland, K. Domen, E. L. Miller, J. A. Turner, H. N. Dinh, *J. Mater. Res.* **2010**, *25* (1), 3–16.
[14] K. Maeda, K. Teramura, K. Domen, *Catal. Surv. Asia* **2007**, *11* (4), 145–157.
[15] G. K. Mor, K. Shankar, M. Paulose, O. K. Varghese, C. A. Grimes, *Nano Lett.* **2005**, *5* (1), 191–195.
[16] S. K. Mohapatra, S. E. John, S. Banerjee, M. Misra, *Chem. Mat.* **2009**, *21* (14), 3048–3055.
[17] J. Goldberger, R. R. He, Y. F. Zhang, S. W. Lee, H. Q. Yan, H. J. Choi, P. Yang, *Nature* 2**003**, 422 (6932), 599–602.
[18] T. Hirai, K. Maeda, M. Yoshida, J. Kubota, S. Ikeda, M. Matsumura, K. Domen, *J. Phys. Chem. C* **2007**, *111* (51), 18853–18855.
[19] K. Maeda, K. Teramura, D. L. Lu, T. Takata, N. Saito, Y. Inoue, K. Domen, *Nature* **2006**, *440* (7082), 295–295.
[20] K. Maeda, D. L. Lu, K. Teramura, K. Domen, *Energy Environ. Sci.* **2010**, *3* (4), 471–478.
[21] D. F. Wang, A. Pierre, M. G. Kibria, K. Cui, X. G. Han, K. H. Bevan, H. Guo, S. Paradis, A. R. Hakima, Z. T. Mi, *Nano Lett.* **2011**, *11* (6), 2353–2357.
[22] K. Maeda, N. Sakamoto, T. Ikeda, H. Ohtsuka, A. K. Xiong, D. L. Lu, M. Kanehara, T. Teranishi, K. Domen, *Chem. Eur. J.* **2010**, *16* (26), 7750–7759.
[23] K. Maeda, H. Hashiguchi, H. Masuda, R. Abe, K. Domen, *J. Phys. Chem. C* **2008**, *112* (9), 3447–3452.
[24] J. F. Geisz, R. C. Reedy, B. M. Keyes, W. K. Metzger, *J. Cryst. Growth* **200**3, 259 (3), 223–231.
[25] C. H. Seager, A. F. Wright, J. Yu, W. Gotz, *J. Appl. Phys.* **2002**, *92* (11), 6553–6560.
[26] I. Shalish, L. Kronik, C. Segal, Y. Rosenwaks, Y. Shapira, U. Tisch, J. Salzman, *Phys. Rev. B* **1999**, *59* (15), 9748–9751.
[27] B. D. Yuhas, D. O. Zitoun, P. J. Pauzauskie, R. R. He, P. Yang, *Angew. Chem. Int. Ed.* **2006**, *45* (3), 420–423.
[28] Y. X. Zhao, E. A. Hernandez-Pagan, N. M. Vargas-Barbosa, J. L. Dysart, T. E. Mallouk, *J. Phys. Chem. Lett.* **2011**, *2* (5), 402–406.

Received: August 24, 2012
Accepted: September 28, 2012
Published online: December 11, 2012

